Earthquakes and Structures, *Vol. 16, No. 2 (2019) 221-234*
DOI: https://doi.org/10.12989/eas.2019.16.2.221

Assessing 3D seismic damage performance of a CFR dam considering various reservoir heights

Memduh Karalar and Murat Çavuşli*

Department of Civil Engineering, Zonguldak Bulent Ecevit University, Zonguldak, Turkey

(Received October 15, 2018, Revised January 21, 2019, Accepted January 23, 2019)

Abstract. Today, many important concrete face rockfill dams (CFRDs) have been built on the world, and some of these important structures are located on the strong seismic regions. In this reason, examination and monitoring of these water construction's seismic behaviour is very important for the safety and future of these dams. In this study, the nonlinear seismic behaviour of Ilısu CFR dam which was built in Turkey in 2017, is investigated for various reservoir water heights taking into account 1995 Kobe near-fault and far-fault ground motions. Three dimensional (3D) finite difference model of the dam is created using the FLAC3D software that is based on the finite difference method. The most suitable mesh range for the 3D model is chosen to achieve the realistic numerical results. Mohr-Coulomb nonlinear material model is used for the rockfill materials and foundation in the seismic analyses. Moreover, Drucker-Prager nonlinear material model is considered for the concrete slab to represent the nonlinearity of the concrete. The dam body, foundation and concrete slab constantly interact during the lifetime of the CFRDs. Therefore, the special interface elements are defined between the dam body-concrete slab and dam body-foundation due to represent the interaction condition in the 3D model. Free field boundary condition that was used rarely for the nonlinear seismic analyses, is considered for the lateral boundaries of the model. In addition, quiet artificial boundary condition that is special boundary condition for the rigid foundation in the earthquake analyses, is used for the bottom of the foundation. The hysteric damping coefficients are separately calculated for all of the materials. These special damping values is defined to the FLAC3D software using the special fish functions to capture the effects of the variation of the modulus and damping ratio with the dynamic shear-strain magnitude. Total 4 different reservoir water heights are taken into account in the seismic analyses. These water heights are empty reservoir, 50 m, 100 m and 130 m (full reservoir), respectively. In the nonlinear seismic analyses, near-fault and far-fault ground motions of 1995 Kobe earthquake are used. According to the numerical analyses, horizontal displacements, vertical displacements and principal stresses for 4 various reservoir water heights are evaluated in detail. Moreover, these results are compared for the near-fault and far-faults earthquakes. The nonlinear seismic analysis results indicate that as the reservoir height increases, the nonlinear seismic behaviour of the dam clearly changes. Each water height has different seismic effects on the earthquake behaviour of Ilısu CFR dam. In addition, it is obviously seen that near-fault earthquakes and far field earthquakes create different nonlinear seismic damages on the nonlinear earthquake behaviour of the dam.

Keywords: concrete face rockfill dam; dam-foundation-concrete slab interaction; free field and quiet boundary condition; near-fault-far-fault earthquake; seismic safety

1. Introduction

Water is vital for people to continue their lives. Mankind has built many water structures (e.g., dams) to benefit from the water from the past to present. There are many dam types on the world in now, and concrete face rockfill (CFR) dams are one of these important hydraulic water structures. Today, these dams are very popular in regions that receive heavy rain, and where impervious soil reserves are insufficient (Cooke 1984). They are used for the flood control, water supply and electricity generation. A CFR dam must be resistant to many external loads during its life (e.g., earthquake loads, hydrostatic pressure). For instance, because of water occupancy rates in the CFRDs change in time, various hydrostatic pressure loads create different effects on the nonlinear behaviour of these water structures in the various periods. In other word, each reservoir height creates different effects on the static and dynamic behaviour of these dams by the effect of the hydrostatic pressure. Moreover, CFR dams that was constructed near causative faults, may undergo strong earthquake loads. The strong ground motions can impose high seismic demand on the CFRD. In this reason, failure of a CFR dam would result in catastrophic social and economic losses. So, when considered the effect of the dynamic and static pressures on the dam behaviour, the investigation of the nonlinear seismic behaviour of the CFR dams considering various reservoir heights is very critical to assess the future and safety of these dams. Many investigators examined the seismic behaviour of CFR dams considering strong ground motions. Bayraktar *et al*. (2009) performed the seismic performance analysis of the Torul Concrete-Faced Rockfill (CFR) Dam that was constructed in Turkey. In the seismic analyses, the horizontal component of the 1992 Erzincan

*Corresponding author, Ph.D.
E-mail: memduhkaralar@beun.edu.tr

http://www.techno-press.com/journals/eas&subpage=7
ISSN: 2092-7614 (Print), 2092-7622 (Online)

earthquake, with a peak ground acceleration of 0.515 g, was used. The earthquake results indicated that the hydrodynamic pressure of reservoir water gives rise to an increase in the maximum displacements and principal stresses of the dam and reduces the earthquake performance of the dam. Moreover, Bayraktar and Kartal (2010) investigated the linear and nonlinear behaviors of a CFR Dam considering the interface elements between concrete slab and rockfill for the seismic analyses. The earthquake analyses were performed for the empty and full reservoir condition of the dam to better see the effect of the reservoir water on the earthquake response of the dam. According to numerical analyses, the displacement and stress components were increased by hydrodynamic pressure. More displacements and stresses were obtained for full reservoir condition when compared the empty condition. Afterwards, Xu *et al*. (2012) developed a finite element procedure to simulate the construction process of the Zipingpu CFRD. A generalized plasticity model was modified to better model the rockfill materials, and the interfaces between face slabs and cushions are modeled using zero thickness interface elements that follow a hyperbolic stress-strain model in the tangential direction. It is seen in this study that the numerical results agree well with in situ monitoring records of dam settlements, indicating that a three-dimensional finite element procedure based on a modified generalized plasticity model and a hyperbolic interface model can be used to evaluate the deformation of CFRDs. Zou *et al*. (2013) employed a 3D dynamic procedure to simulate the dynamic responses of the Zipingpu CFRD. Dam deformation, face-slab stress and face joint dislocations were simulated. The results were compared with the field measurements. The results of this study indicate that a 3D finite element procedure based on a generalized plasticity model can be used to evaluate the dynamic responses of CFRDs during strong earthquakes. Then, Xu *et al*. (2016) investigated the effects of hydrodynamic pressure on the face slab response of a 300 m high CFRD under strong earthquake loads. The distribution of the hydrodynamic pressure and the mechanism are examined in detail. In addition, it is revealed that hydrodynamic pressure influences the dynamic stress in face slabs through the frictional force between the cushion and the slabs, and it cannot be ignored in the seismic analysis of a concrete face rockfill dam. Han *et al*. (2016) investigated the seismic response of Yele dam using finite element method. The results showed that the predicted seismic deformation of the Yele dam is in agreement with field observations that suggested that the dam operated safely during the Wenchuan earthquake. Cen *et al*. (2016) simulated the seismic response of a 100 m high concrete face rockfill dam (CFRD) using the three-dimensional finite element method. The calculated results showed that the number of damaged and cracking elements on concrete slabs grows with the duration of earthquakes. With increasing earthquake intensity, the damaged zone and cracking zone on concrete slabs grow wider. In addition, Chen *et al*. (2016) examined the seismic responses of the Zipingpu concrete face rockfill dam using the finite element method. Numerical results show that the input accelerations were considerably amplified near the top of the dam and the strong shaking resulted in considerable settlement of the rockfill materials, with a maximum value exceeding 90 cm at the crest. Zou *et al*. (2018) selected 16 ground motions for seismic failure analyses of a CFR dam for numerical analyses, and these ground motions include 8 pulse like motions with rupture forward directivity effects and 8 non-pulse motions. The rockfill materials are described using a generalized plasticity model. In addition, the interfaces between the face slabs and cushions are modelled using interface elements. The numerical analysis results indicate that although the near-fault pulse like ground motion has a moderate impact on the dam acceleration, it has a remarkable impact on the residual deformation of dam and concrete slab damage, especially for the dam crest. Afterwards, Xu *et al*. (2018) established a method to calculate the nonlinear dynamic interactions of CFRD, and it is indicated that water compressibility can significantly affect the stress in the face slabs. In addition, many investigators examined the nonlinear seismic behaviour of the CFR rockfill dams under effect of the strong ground motions, and the effect of the strong ground motions on the nonlinear behaviour was discussed in detail (Bayraktar *et al*. 2011, Dakoulas 2012, Kong *et al*. 2017, Noorzad and Omidvar 2010, Seiphoori *et al*. 2011, Xu *et al*. 2014, Xu *et al*. 2015, Yamaguchi *et al*. 2012).

Both far-fault and near-fault earthquakes can cause major damages in the CFR dam body, and when investigated the literature, very few investigators examined the effects of reservoir water height on the nonlinear seismic behaviour of the CFR dams considering the near and far-fault earthquakes. For this reason, 4 different water heights (empty reservoir condition, 50 m, 100 m and 130 m) are used in the seismic analyses taking into account 1995 Kobe near and far-fault earthquakes in this work. 4 various numerical analyses are performed for 4 different reservoir water heights, and these numerical results are compared with each other. Because of subject of this study was rarely studied in the past, this work is very important to evaluate the effect of the reservoir water height on the seismic performance of the CFR dams. Moreover, free field and quiet seismic boundary conditions that were rarely used in the past to examine 3D behaviour of the CFR dams, are taken into account to examined the 3D nonlinear seismic behaviour of Ilısu CFR dams. Thus, this work is vital for filling these deficiencies in the literature. According to the 3D finite difference analyses, horizontal displacements, vertical displacements and principal stresses for 5 various nodal points on the dam body surface are assessed in detail.

2. General descriptions of the ilısu hydraulic project

2.1 Project location and geology

The Ilısu Dam was completed in 2017 year, and the project area is 117 km away from the center of Mardin province. Dam was built on the strong seismic zone in Turkey, and it is part of the Southeastern Anatolian Project (GAP). This structure is the largest hydropower project in

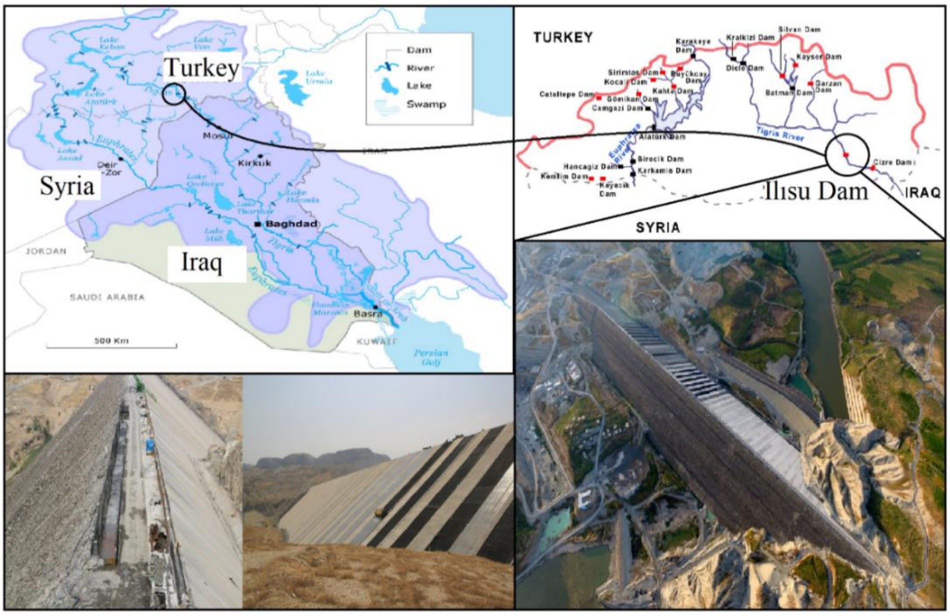

Fig. 1 General view of Ilısu dam (DSI 2018)

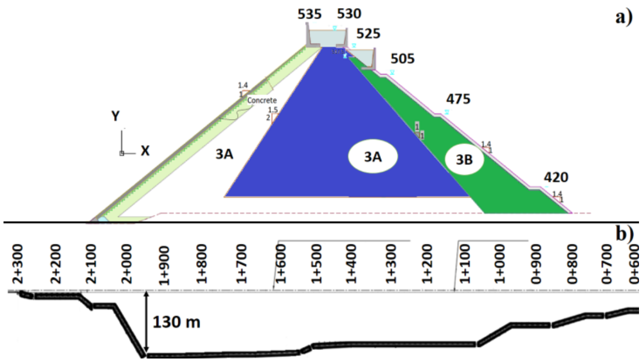

Fig. 2 (a) The typical cross section of Ilısu dam; (b) Changing of the dam body depth along crest axis (DSI 2018)

Turkey, and it is the longest concrete faced rockfill dam (1775 m) in the world (Fig. 1).

The project includes totally 44 million m^3 filling material. It has 3 diversion tunnels with a diameter of 12 m and length of 1 km. Dam's precipitation area is 35509 km^2. The crest width is 8 m. Dam body height is 130 m. The lake volume is 10.4 billion m^3. Maximum water elevation is 526.82 m, and reservoir area is 318.5 km^2. The project generates 3.833 GWh power per year in average with an installed capacity of 1.200 MW. Ilısu dam's location is showed in detail in Fig. 1. The slopes of the upstream side and downstream side of the Ilısu dam are 1:1.4, and slopes of the transition zones are 2:1.5. The typical cross section of Ilısu dam and details of the dam body height are demonstrated in Fig. 2. Moreover, geology of Ilısu hydraulic project is shown in Fig. 3. According to Fig. 3, there are 6 various rockfill materials around the dam project zone. These rockfill materials are limestone, clayey/marley limestone, siltstone/claystone, sandstone/marl, marly/ limestone and basalt. Many of these rockfill materials are used to construct the body of Ilısu dam (e.g., basalt, limestone).

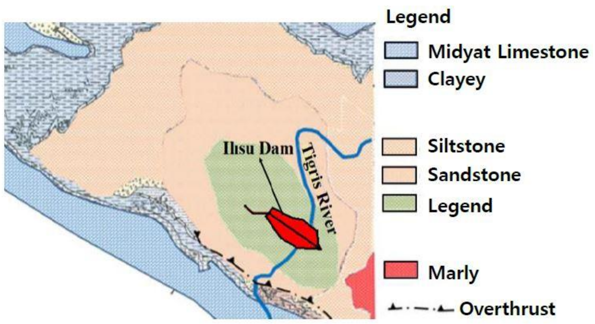

Fig. 3 Geology of Ilısu hydraulic project

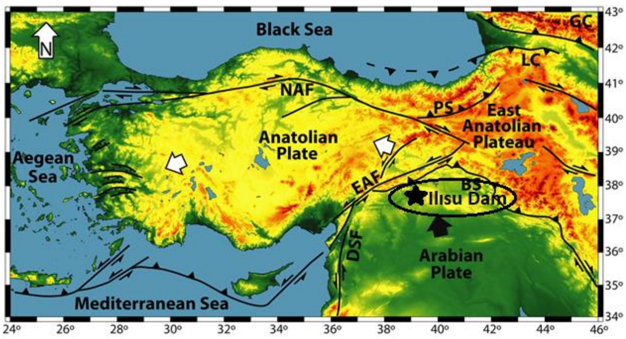

Fig. 4 The fault map of Turkey and location of the Ilısu dam in seismic faults

2.2 Seismicity of the zone

Turkey is located in one of the most actively deforming regions in the world. The tectonic faults in Turkey depends on relative motions among the African, the Aegean, the Arabian, the Anatolian, the Black Sea and the Eurasian plates. The neotectonics of Turkey is directed by three major elements: a) The Aegean-Cyprean Arc, a convergent plate boundary where the African Plate to the south is beneath the Anatolian Plate to the north; b) The North Anatolian Fault (NAF) Zone; c) The East Anatolian Fault

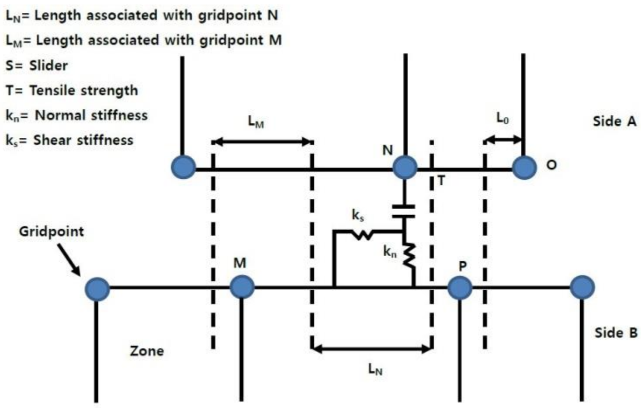

Fig. 5 An interface condition between A and B sides (Itasca 2002)

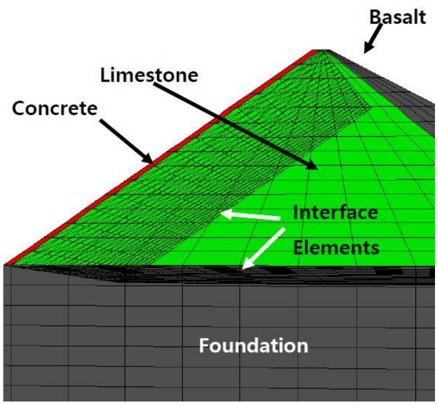

Fig. 6 Interface conditions between dam body-foundation and dam body-concrete slab of the Ilısu dam

(EAF) zone (Fig. 4). The East Anatolian Fault Zone (EAFZ) represents a plate boundary extending over 500 km between the Arabian and Anatolian plates. It is one of the largest currently active continental strike slip faults in the world. Relative plate motion occurs with slip rates ranging from 6 to 10 mm/year, and has resulted in destructive earthquakes in eastern Turkey as documented by historical records. In addition, there have been large magnitude (M>7) earthquakes in the EAF zone. It was showed in Fig. 4 in detail. Moreover, the Ilısu dam was built very close to the East Anatolian Fault (EAF). Due to its long and extensive historical record, the EAF zone provides an important natural laboratory to understand earthquake mechanics and fault behaviour over multiple earthquake cycles. Although the long historical record of the region, all historical earthquakes records for the East Anatolian Fault zone is not yet available.

3. Mathematical formulation of the interaction condition between discrete surfaces

Interaction condition is very critical for huge water structures such as CFR dams. This situation occurs between the dam body, foundation and concrete slab for the CFR dams. In FLAC3D software, the interaction condition is represented defining the interaction stiffness values between the discrete surfaces as seen in Fig. 5 and Fig. 6.

FLAC3D utilizes a special contact logic that is used in the different element methods, to represent interaction condition for either side of the interface. As seen in Fig. 5, grid point N is controlled for the contact situation between grid points M and P. If this contact condition is realized, the normal vector (n) is computed for the grid point N. In addition, length (L) for the contact at the point N along the interface is described. L represents the half of the nearest grid point's distance to grid point N. In this method, the interface is divided into contiguous segments, and each segment is checked by a grid point. For time step, the velocity ($\dot{u}_i$) of grid points is stated as seen at Equal 1. Since the velocity's unit is displacement for time step, and the calculation of the time step is scaled to unity to speed convergence. The displacement for each time step is

$$\Delta u_i \equiv u_i \tag{1}$$

A contact point's displacement vector is resolved for the normal and shear directions, and total forces (normal and shear) are determined as below (Eq. (2)).

$$\begin{aligned} F_n^{(t+\Delta t)} &= F_n^{(t)} - k_n \Delta u_n^{(t+(1/2)\Delta t)} L \\ F_s^{(t+\Delta t)} &= F_s^{(t)} - k_s \Delta u_s^{(t+(1/2)\Delta t)} L \end{aligned} \tag{2}$$

Normal (k_n) and shear (k_s) stiffness values are very different for each interface surface. Unit of the k_n and k_s stiffness is stress/displacement (Itasca 2002). In this study, k_n and k_s stiffness are separately calculated for each discrete surface. These stiffness values are considered as 10^8 Pa/m between the dam body and foundation. Moreover, these values are taken into account as 10^9 Pa/m between the dam body and concrete slab (Karalar and Çavuşli 2018). Shear and normal stiffness values are defined to FLAC3D software using special fish functions.

Normal and shear stiffness (k_n and k_s) are not well-known parameters, and they are not easily calculated. Many numerical procedures have been derived in the past, and two important methods are generally used in the interaction analyses. One of them is based on the rock mass's deformation properties, and second one is derived from the joint infilling material's properties. These procedures are explained in detail as seen below.

3.1 Calculation of normal and shear stiffness considering rockfill properties

$$\frac{1}{E_m} = \frac{1}{E_i} + \frac{1}{k_n L} \tag{3}$$

In Eq. (3), E_m is modulus of rock mass; E_i is intact rock modulus; k_n is joint normal stiffness; and L is mean joint spacing. Eq. (3) can be rearranged to obtain the joint normal stiffness as given in Eq. (4).

$$k_n = \frac{E_i E_m}{L(E_i - E_m)} \tag{4}$$

The same expression may be considered to derive a relation for the joint shear stiffness as see at Eq. (5).

$$k_s = \frac{G_i G_m}{L(G_i - G_m)} \tag{5}$$

In Eq. (5), G_m is rock mass shear modulus; G_i is intact rock shear modulus; and k_s is joint shear stiffness. When the equivalent continuum assumption is extended to three orthogonal joint sets, it is obtained the following relations.

$$E_a = \left(\frac{1}{E_i} + \frac{1}{L_a k_{na}}\right)^{-1} (a = 1,2,3)$$
$$G_{ab} = \left(\frac{1}{G_i} + \frac{1}{L_a k_{sa}} + \frac{1}{L_b k_{sb}}\right)^{-1} (a, b = 1,2,3) \tag{6}$$

Many equals have been acquired for 2D and 3D characterizations.

3.2 Calculation of normal and shear stiffness considering infill rockfill properties

Second procedure for forecasting the stiffness of joint presumes that an interaction joint has an infill material. The joint stiffness can be evaluated from the infilling material by the following equation.

$$k_n = \frac{E_0}{h}$$
$$k_s = \frac{G_0}{h} \tag{7}$$

In Eq. (7), k_s is joint shear stiffness; k_n is joint normal stiffness; G_o is shear modulus of infill material; E_o is Young's modulus of infill material, and h is joint thickness or opening.

4. Mohr-Coulomb material model

This nonlinear material model is generally used for many rockfill materials in the FLAC3D software. The implementation of Mohr Coulomb material model is given as following: σ_1, σ_2, σ_3 are utilized for the out of plane stress. The principal directions and principal stresses are assessed from the components of stress tensor.

$$\sigma_1 \le \sigma_2 \le \sigma_3 \tag{8}$$

Δe_1, Δe_2, Δe_3 are defined as seen below.

$$\Delta e_i = \Delta e_i^e + \Delta e_i^p \qquad i: 1, 2, 3 \tag{9}$$

In Eq. (9), e and p; elastic part and plastic part. The plastic parts are nonzero only during plastic flow (Itasca 2002). Hooke's law for principal stress and principal strain is as seen below

$$\Delta\sigma_1 = \alpha_1 \Delta e_1^e + \alpha_2 \left(\Delta e_2^e + \Delta e_3^e\right) \tag{10}$$

$$\Delta\sigma_2 = \alpha_1 \Delta e_2^e + \alpha_2 \left(\Delta e_1^e + \Delta e_3^e\right) \tag{11}$$

$$\Delta\sigma_3 = \alpha_1 \Delta e_3^e + \alpha_2 \left(\Delta e_1^e + \Delta e_2^e\right) \tag{12}$$

where $\alpha_1 = K + 4G/3$ and $\alpha_1 = K - 2G/3$

Potential and yield functions are presented as below in detail.

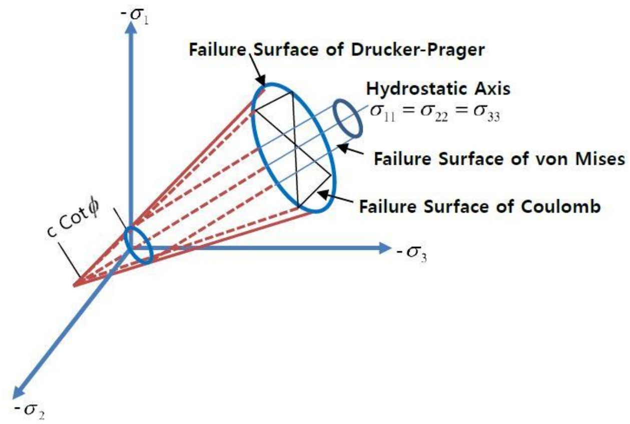

Fig. 7 Mohr-Coulomb failure criterion (Itasca 2002)

According to Eq. (13), the failure criterion can be defined in the plane as seen in Fig. 7. The failure envelope is considering from point A to B

$$f^s = \sigma_1 - \sigma_3 N\phi + 2c\sqrt{N\phi} \tag{13}$$

From point B to C by a tension yield function

$$f^t = \sigma^t - \sigma_3 \tag{14}$$

In Eq. (13) and (14), c is the cohesion, ϕ is the friction angle, σ_t the tensile strength and

$$N_\phi = \frac{1 + \sin\phi}{1 - \sin\phi} \tag{15}$$

$$\sigma_{\max}^t = \frac{c}{\tan\phi} \tag{16}$$

g^s (the shear potential function) represents a flow rule

$$g^s = \sigma_1 - \sigma_3 N_\Psi \tag{17}$$

In Eq. (17), ψ; the dilation angle

$$N_\Psi = \frac{1 + \sin\Psi}{1 - \sin\Psi} \tag{18}$$

The flow rule that associates of tensile failure is derived from the potential function g^t

$$g^t = -\sigma_3 \tag{19}$$

The flow rules for 3D dam model are described a unique definition in the vicinity of an edge of the composite yield function in three-dimensional stress space by application of a technique, illustrated below, for the case of a shear-tension edge. A function, $h(\sigma_1, \sigma_3)=0$, which is represented by the diagonal between the representation of $f^s=0$ and $f^t=0$ in the (σ_1, σ_3) plane, is defined (in Fig. 8). This function has the form

$$h = \sigma_3 - \sigma^t + \alpha^P\left(\sigma_1 - \sigma^P\right) \tag{20}$$

In Eq. (20), α^p and σ^p defined as below

$$\alpha^P = \sqrt{1 + N_\phi^2} + N_\phi \tag{21}$$

and

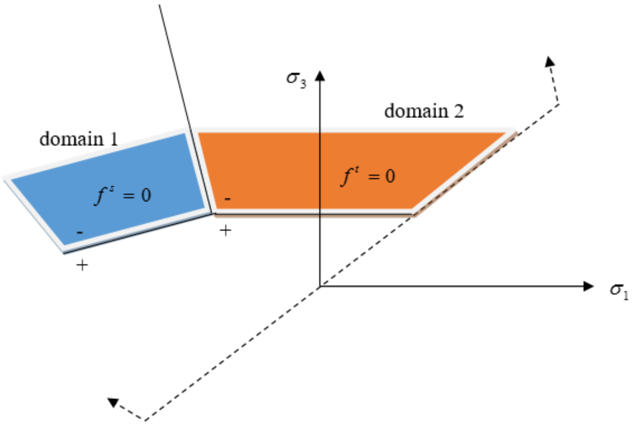

Fig. 8 Mohr-Coulomb model: domains used in the definition of the flow rule (Itasca 2002)

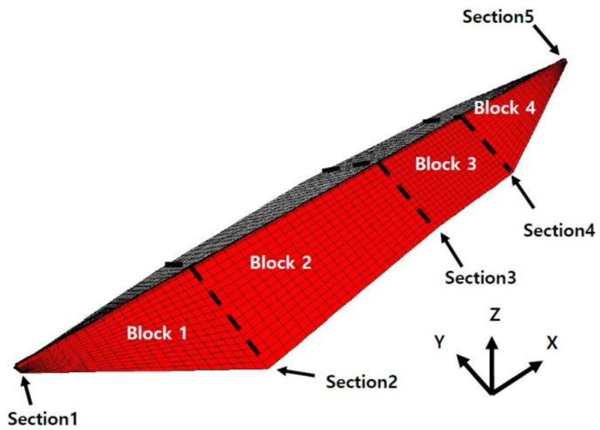

Fig. 9 View of the section and blocks in the 3D finite difference model

$$\sigma^P = \sigma^t N_\phi - 2c\sqrt{N_\phi} \tag{22}$$

5. Finite difference model and material properties of ilisu dam

While creating the 3D finite difference model of Ilısu dam, all rockfill materials, and concrete slab that is built to hinder the leakage in the dam body are modelled as the original project of the dam. The 3D model of the dam body has 5 different sections, and these section's geometrical properties are very different from each other. Each section has different heights along the dam body. While modelling Ilısu dam, these different sections are merged, and finite difference model of the dam body is created. 3D finite difference model of the dam body has 4 various blocks. Details of the sections, and blocks are presented in the Fig. 9.

After the three dimensional model of dam body is modelled, the foundation and reservoir water are created in detail. While modelling the foundation, foundation is extended toward downstream and the valley side as much as dam height. Also, it is extended three times of the dam height at up-stream side of dam. Finally, height of the foundation is considered as much as the dam height. These

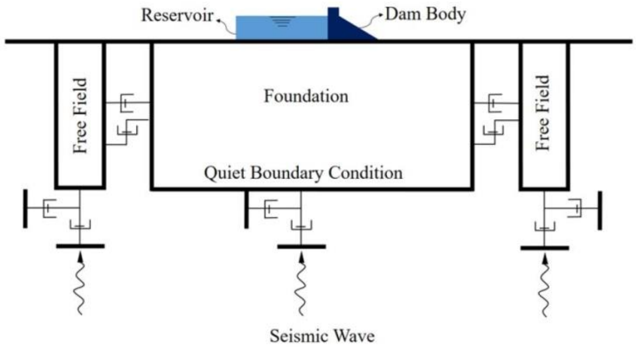

Fig. 10 Boundary conditions for the 3d finite difference model

lengths and heights are the most critical conditions for the seismic analyses of the dams (Kartal *et al*. 2017). Total 1104547 finite difference elements are used in 3D finite difference model. Mohr Coulomb material model and Drucker Prager material model which are special nonlinear material models, are used for the rockfill material foundation and concrete slab, respectively. Special fish functions are used while defining the material model to the FLAC3D software. Moreover, special interface elements are defined between the rockfill material-foundation and the concrete slab-rockfill material to provide interaction condition between the discrete surfaces. Hysteretic damping models are usually employed to characterize damped dynamic properties of nonlinear mechanical systems. Various hysteretic damping models are calculated for all materials (rockfill materials, concrete slab and foundation) due to all materials have different characteristic properties. While defining these hysteric damping models to FLAC3D software, special fish functions are written and defined to the FLAC3D software. Free field boundary condition that is special boundary condition for seismic analyses, is defined to the lateral boundaries of the 3D finite difference model for seismic analyses. This boundary condition is available for only lateral boundaries as seen Fig. 10, and it is made up of a combination of a load history and a viscous boundary.

These boundaries allow for an input of an earthquake motion while still absorbing incoming waves. In addition, quiet boundary (viscous boundary) condition is used for the bottom of the 3D model in the nonlinear earthquake analyses. Free field and quiet boundary conditions for the 3D finite difference model of Ilısu dam are shown in Fig. 11 in detail.

Afterwards, the reservoir water is modelled considering the effect of the leakage in the dam body. Water height is taken into account as empty water condition, 50 m, 100 m, 130 m of the reservoir water height, respectively. While creating the reservoir water, water loads are calculated for each nodes of the dam's upstream side considering hydrostatic ware pressure. Then, water table for 4 various reservoir water heights is defined to the FLAC3D software using the special fish function to provide the leakage condition in the dam body. The creating and meshing of the three dimensional model of Ilısu dam took very long time. This process is not automated, and so each process is individually calculated. Many problems and errors are

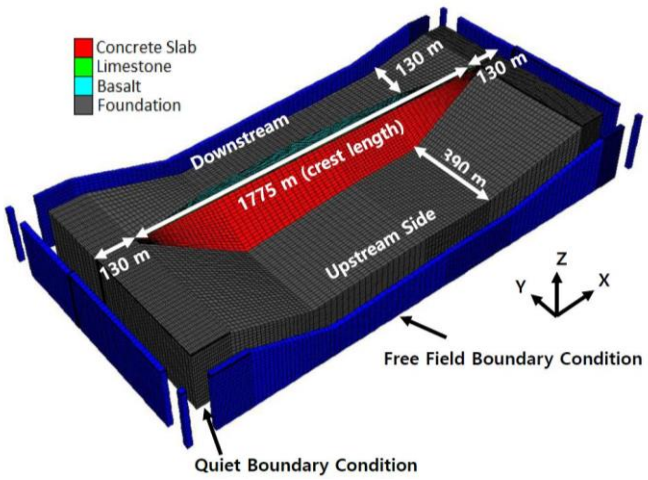

Fig. 11 3D finite difference model of Ilısu CFR Dam

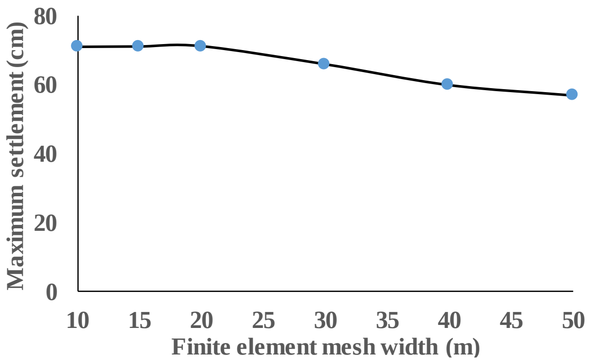

Fig. 12 Settlement changes of the crest for different mesh widths

Table 1 Material properties of Ilısu CFR dam (DSI, 2018)

Characteristics	Specify weight	Unit Weight	Porosity	Water content	Air content	Material content
Unit	g/cm^3			%		
2B	2.74	2.23	18.61	4.05	14.56	81.39
3A	2.68	1.99	25.75	7.78	17.97	74.25
3B	3.01	2.25	25.25	1.50	23.75	74.75

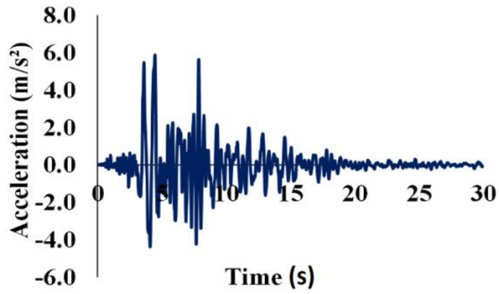

(a) Near-fault accelerogram

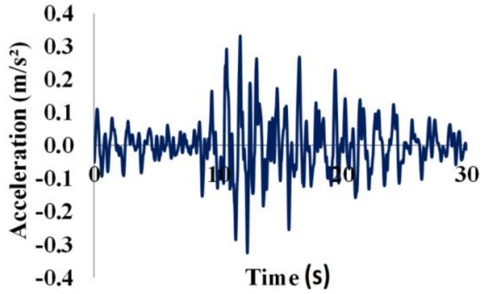

(b) Far-fault accelerogram

Fig. 13 Near-fault and far-fault accelerogram for 1995 Kobe earthquake

encountered during nonlinear seismic analyses due to three-dimensional finite difference model of the Ilısu dam has a great number of nodes and elements. So, the 3D mesh is changed many times, and a new mesh is modelled so that the correct result can be achieved, and the program will not fail. While analysing the Ilısu dam, total 6 different mesh widths are created to find the correct mesh width. These widths are 10 m, 15 m, 20 m, 30 m, 40 m, 50 m, respectively. It is seen from numerical analyses that the maximum settlements on the crest of the dam do not change for less mesh width than 10 m (Fig. 12). So, mesh width is selected 10 m for seismic analyses.

The Ilısu CFR dam was constructed as concrete faced rockfill dam, and it was built using many various rockfill materials such as basalt (3B), limestone (3A) and bedding zone (2B). In addition, all rockfill materials have different mechanical properties. Mechanical properties of the rockfill materials are selected from the laboratory experiments for earthquake analyses as given in Table 1. Moreover, while constructing the Ilısu dam, these rockfill materials were compacted by sheepsfoot rollers.

6. Nonlinear seismic analysis results

Water occupancy rates of the concrete face rockfill dams change from the season to season. Each water occupancy rate creates different effects on the nonlinear seismic behaviour of the CFR dams depending hydrostatic pressure. In this reason, when considered CFR dams that were constructed on the strong seismic zone, the effect of the reservoir water height on the nonlinear seismic behaviour of the dam is very important for the safety and future of the dam. In this study, the nonlinear seismic behaviour of Ilısu dam is investigated graphically taking into account 1995 Kobe near-fault and far-fault earthquakes. Three components (x, y, z) of near-fault and far-fault earthquake are presented in Fig. 13. As seen Fig. 13, duration of both earthquakes is 30 seconds. Maximum acceleration of the near-fault earthquake is 6.05 m/s^2, and it occurred at 4.1th second of the earthquake. Moreover, maximum acceleration of the far-fault earthquake is 0.36 m/s^2, and it occurred at 11.9th second of the earthquake for far-fault earthquake.

While performing earthquake analyses, principal stresses and displacements that are obtained from the static condition of the dam were not ignored. In other word, before performed the seismic analyses for all reservoir water heights, all displacements (vertical and horizontal) and principal stresses that are obtained from the collapsed 3D model, are set to zero in order to exclude the stresses and deformations. Moreover, interaction elements should be defined between the dam body-foundation-concrete slab to provide interaction between the discrete surfaces. Special shear (k_s) and normal (k_n) stiffness coefficients are

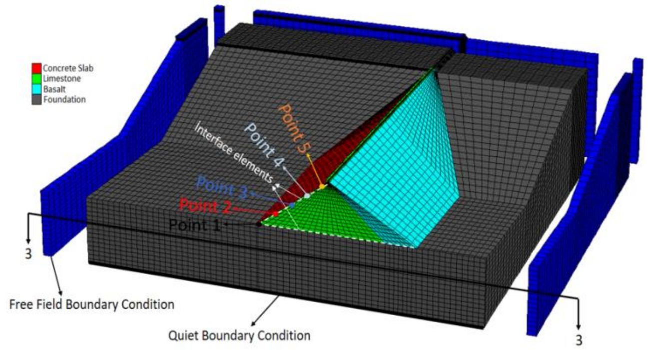

Fig. 14 View from section 3-3 of the finite difference model of Ilısu Dam

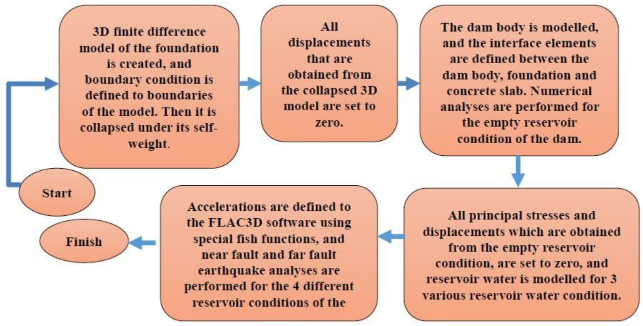

Fig. 15 Numerical analysis algorithm for nonlinear seismic analyses

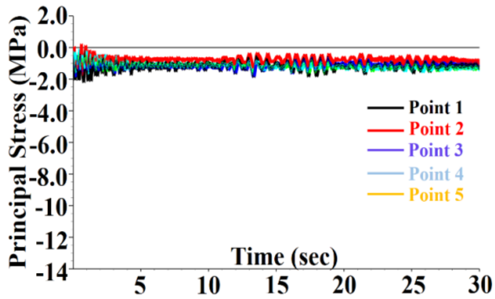

(a) Far-fault earthquake analysis results

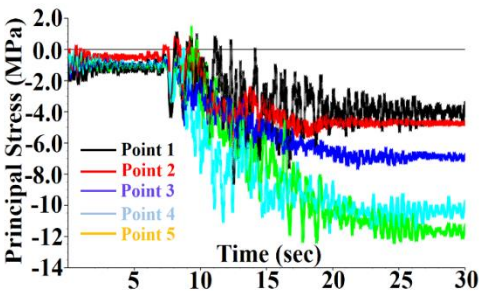

(b) Near-fault earthquake analysis results

Fig. 16 Principal stress results for empty reservoir condition

calculated according to the mechanical properties of each rockfill material in this study. These coefficients and special friction values are defined between these discrete surfaces to provide the interaction condition using the special fish functions. Normal shear stiffness and friction values between dam body and foundation are considered as 10^8 Pa/m and 30°, respectively. In addition, it is considered 10^9 Pa/m between the concrete slab and dam body (Karalar and Çavuşli 2018). While determining the seismic boundary conditions of the 3D model, the special boundary conditions that are special for the nonlinear seismic analyses, are used for the seismic analyses. Quiet boundary condition is defined for the bottom of the foundation to represented the viscous boundary condition. Moreover, the free field boundary condition is used for the lateral surfaces of the 3D model. Accelerations and durations of the earthquakes are defined to FLAC3D software using special fish functions, and these acceleration values are applied to the bottom of the 3D model considering *x*, *y* and *z* directions of the earthquake. Nonlinear seismic analyses are performed for 4 various reservoir heights. These reservoir water heights are empty condition, 50 m, 100 m and 130 m (full reservoir condition), respectively. As a result of the seismic analysis, the principal stresses, horizontal displacements and vertical displacements are presented and assessed graphically for five critical nodal points on the dam body surface, and fatigue in the rockfill materials are evaluated in detail. These nodal points on the dam body surface are shown in Fig. 14, and numerical analysis algorithm for seismic analyses is shown in Fig. 15.

6.1 Principal stress results

When considered the huge water structures such as CFR dams, investigation of effect of reservoir water height on the seismic principal stress behaviour of these dams is very important to evaluate the future and safety of such hydraulic structures. In this section, the principal stress behaviour of Ilısu CFR dam is examined and assessed for four various reservoir water heights considering 1995 Kobe near-fault and far-fault earthquakes. Nonlinear seismic analysis results are shown in Figs. 16-19 in detail. According to Fig. 16, principal stress results for the empty reservoir condition of Ilısu dam is presented, and analysis results are compared for the near-fault and far-fault earthquakes. When these earthquakes are compared with each other, very significant seismic stress differences are observed on the dam body surface (as seen Fig. 16(a) and 16(b)). According to Fig. 16(a), stress results for empty reservoir condition are graphically presented taking into account far-fault earthquake. As all nodal points are compared with each other, very close principal stress results are obtained for each point. Minimum principal stress value is acquired at Point 2, and its numerical value is approximately 1.5 MPa. Moreover, maximum stress occurred at Point 5, and its numerical value is about 2 MPa as seen Fig. 16(a). In Fig. 16(b), principal stress results for empty reservoir condition are shown considering Kobe near-fault earthquake. Very important stress changes are obtained for the near-fault earthquake when compared the far-fault earthquake. Maximum principal stress value is observed at Point 5, and its numerical value is 12.3 MPa. In addition, minimum stress value is obtained at Point 1. No significant stress values occurred during first 10 seconds of the earthquake for all nodal points. In Fig. 17(a), principal stress results are presented for 50 m of the reservoir water height considering far-fault earthquake. Because of Point 1 expose to the

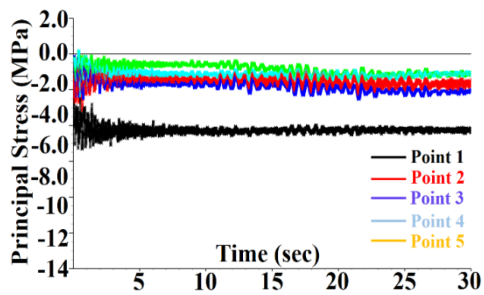

(a) Far-fault earthquake analysis results

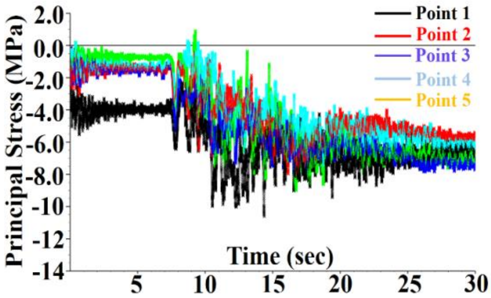

(b) Near-fault earthquake analysis results

Fig. 17 Principal stress results for 50 m of the reservoir water height

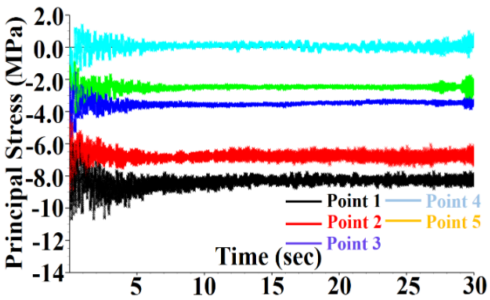

(a) Far-fault earthquake analysis results

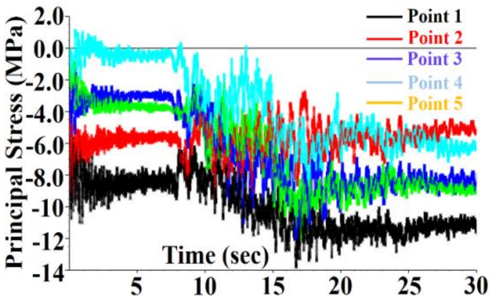

(b) Near-fault earthquake analysis results

Fig. 18 Principal stress results for 100 m of the reservoir water height

maximum hydrostatic pressure, 4.9 MPa maximum stress value is observed at Point 1 (the lowest point), and minimum stress occurred at Point 5 (top point). According to Fig. 17(b), more principal stress values are obtained for near-fault earthquake compared far-fault earthquake. 10.2 MPa maximum principal stress is observed at Point 1 due to more hydrostatic pressure affects this nodal point. Moreover, minimum principal stress occurred at Point 5 as seen Fig. 17(b). As compared Fig. 16 and Fig. 17, the effect of the reservoir water height on the seismic behaviour of the

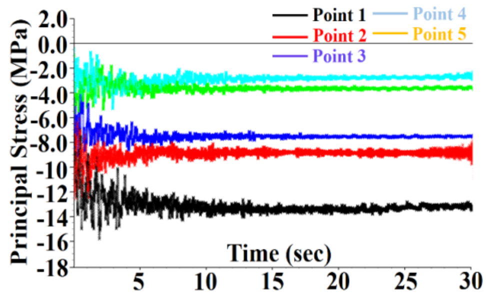

(a) Far-fault earthquake analysis results

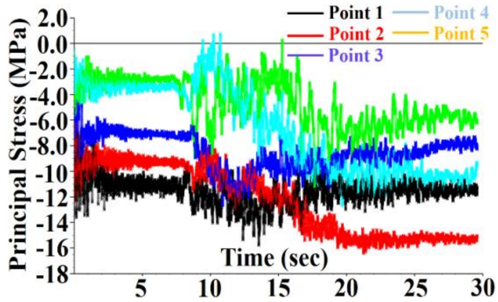

(b) Near-fault earthquake analysis results

Fig. 19 Principal stress results for 130 m of the reservoir water height

Ilısu CFR dam is clearly seen.

In Fig. 18, principal stress results are shown for 100 m of the reservoir water height. As examined Fig. 18(a), it is obviously seen that when reservoir water height increases, the nonlinear seismic behaviour of Ilısu CFR dam significantly changes. Maximum principal stress value occurred at Point 1, and its numerical value is 7.8 MPa. In addition, minimum stress is observed at Point 4 for far-fault earthquake as seen Fig. 18(a). For Point 4, negative principal stress values are observed at the certain section of the time history analysis. In Fig. 18(b), near-fault earthquake results are presented for 100 m of the reservoir water height. 13.7 MPa maximum stress value is observed at Point 1 at 16.6th second of the Kobe near-fault earthquake. Minimum stress occurred at Point 4, and no significant stress values are observed during first 8 seconds of the earthquake. After 8th second of the earthquake, very important stress differences are observed for five critical nodal points (Fig. 18(b)). In Fig. 19(a), far-fault seismic analysis results are shown for 130 m of the reservoir water height (full reservoir condition). Approximately 16 MPa maximum principal stress is observed at Point 1 at 2.3th second of the earthquake. In addition, minimum stress value occurred at Point 4, and very close stress values are observed for Point 4 and Point 5 (Fig. 19(a)). In Fig. 19(b), near-fault earthquake analysis results are presented for 130 m of the reservoir water height. The most critical stress results are acquired for this reservoir condition. 16.4 MPa maximum principal stress value is observed at Point 2, and minimum stress occurred at Point 4. When compared 4 various reservoir water heights of Ilısu dam, maximum stress values are observed at the full reservoir condition (130 m). It is clearly understood from these principal stress results that reservoir water height significantly alters the seismic behaviour of the CFR dams. Moreover, near-fault

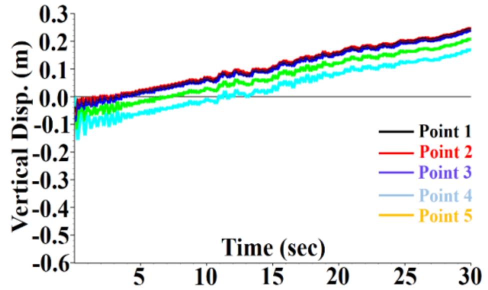

(a) Far-fault earthquake analysis results

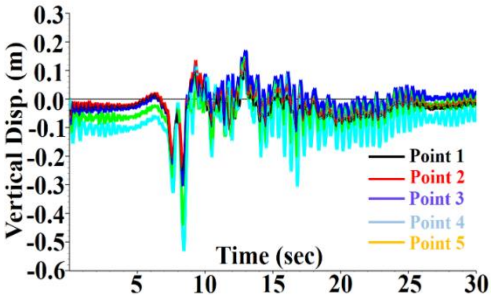

(b) Near-fault earthquake analysis results

Fig. 20 Vertical displacement results for empty reservoir condition

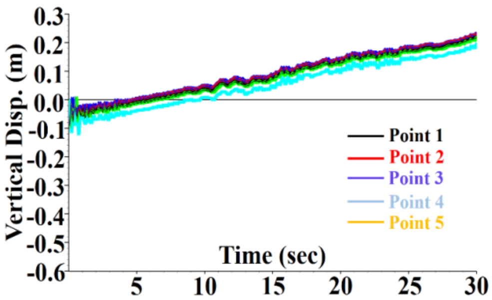

(a) Far-fault earthquake analysis results

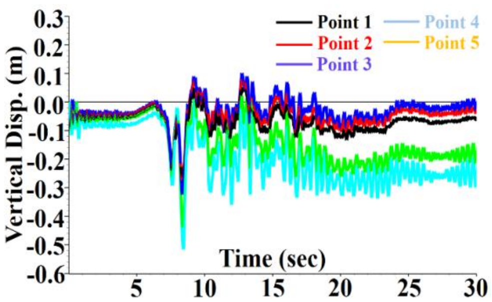

(b) Near-fault earthquake analysis results

Fig. 21 Vertical displacement results for 50 m of the reservoir water height

earthquakes have more seismic effects on the nonlinear stress behaviour of CFR dams than far-fault earthquakes.

6.2 Vertical displacement results

Vertical displacements that occur on the dam body surface during the strong earthquakes, may be very dangerous for the safety of the CFR dams. So, each CFR dam's vertical displacement behaviour must continuously have examined taking into account seismicity of the zone.

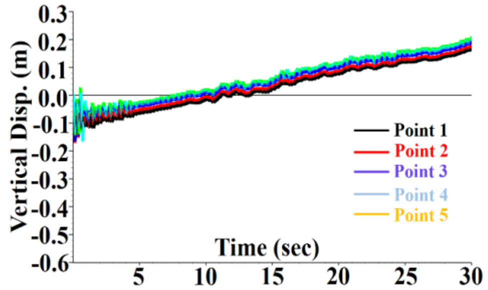

(a) Far-fault earthquake analysis results

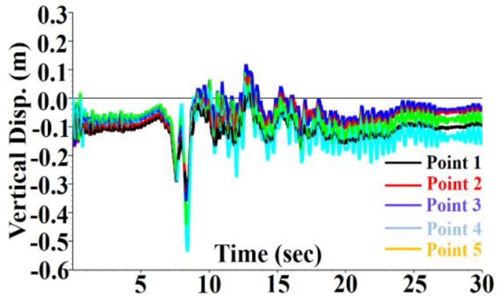

(b) Near-fault earthquake analysis results

Fig. 22 Vertical displacement results for 100 m of the reservoir water height

In this section, the effect of reservoir water height on the nonlinear vertical displacement behaviour of the Ilısu CFR dam is investigated considering 1995 Kobe near-fault and far-fault earthquakes. Numerical analysis results are shown in Figs. 20-23 in detail. When investigated these numerical results, it is obviously seen that significant vertical displacement differences are observed for 4 various reservoir water heights. In Fig. 20(a), vertical displacement results for the empty reservoir condition are presented considering the far-fault earthquake. During first 5 seconds, the vertical displacement direction of the nodal points is negative, and the direction of the displacements changed after this second. -0.16 m maximum vertical displacement value is observed at Point 4. In addition, maximum displacement in positive direction occurred at Point 2 as seen Fig 20(a). This result is shown that different vertical displacements occur during earthquake on the dam body surface. In Fig. 20(b), vertical displacement results for empty water condition are presented for near-fault earthquake. As compared with the far-fault earthquake condition, more displacements occurred for the near-fault earthquake. -0.54 m maximum vertical displacement is observed at Point 4, and minimum displacements occurred at Point 2. According to Fig. 21, vertical displacements for 50 m of the reservoir water height are shown considering near-fault and far-fault. In Fig. 21(a), -0.13 m maximum vertical displacement is observed at Point 4, and maximum displacement in positive direction occurred at Point 3. In addition, near-fault earthquake results for 50 m water height are shown in Fig. 21(b). Maximum vertical displacement is observed at Point 4, and its numerical value is -0.52 m. When compared Fig. 20(b) and Fig. 21(b), more displacements occurred for 50 m of the reservoir water height for all nodal points. This result is clearly shown the effect of the hydrostatic pressure on the seismic vertical

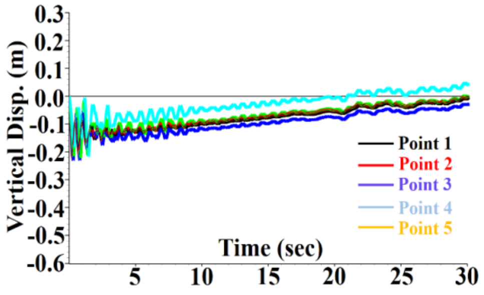

(a) Far-fault earthquake analysis results

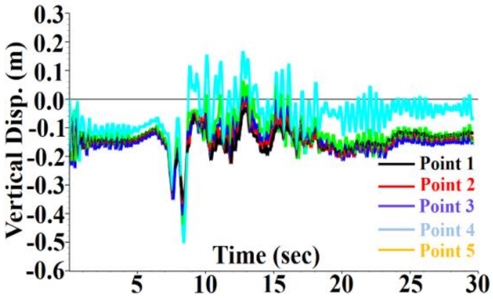

(b) Near-fault earthquake analysis results

Fig. 23 Vertical displacement results for 130 m of the reservoir water height

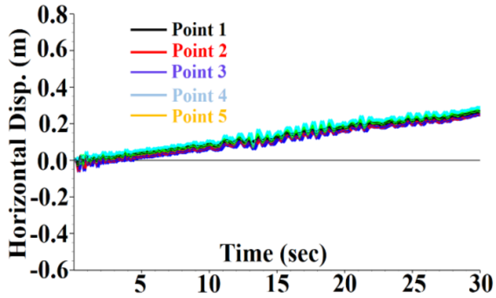

(a) Far-fault earthquake analysis results

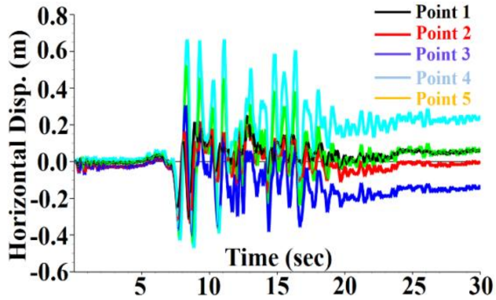

(b) Near-fault earthquake analysis results

Fig. 24 Horizontal displacement results for empty reservoir condition

displacement behaviour of Ilısu CFR dam.

In Fig. 22, vertical displacement results for 100 m of the reservoir water height are graphically shown considering far-fault and near-fault earthquakes. When examined Fig. 22(a) (far-fault earthquake analysis results), maximum displacements in the positive direction occurred at Point 1, and maximum vertical displacements in negative direction are observed for Point 5. In Fig. 22(b), vertical displacements are presented for the near-fault earthquake. -0.55 m maximum displacement is observed at Point 4, and minimum displacement occurred at Point 3. As compared Fig. 20(b), 21(b) and 22(b), more vertical displacement values are obtained for all nodal points in Fig. 22(b). According to Fig. 23, vertical displacements for 130 m of the reservoir water height (full reservoir condition) are presented taking into account far-fault and near-fault earthquakes. In Fig. 23(a), -0.23 m maximum vertical displacement is observed at Point 3 (middle point), and minimum displacement occurred at Point 4. This result is shown that the maximum vertical displacements occur at approximately middle section of the dam body surface for the full reservoir condition during the earthquake. In Fig. 23(b), vertical displacements for 130 m of the reservoir water height are shown taking into account near-fault earthquake. During the earthquake, -0.54 m maximum displacement is observed Point 4, and minimum displacements occurred at Point 3. When all vertical displacement analyses are compared with each other, it is clearly seen the effect of the hydrostatic pressure on the nonlinear settlement behaviour of Ilısu dam. In addition, near-fault earthquake has more nonlinear seismic effects on the nonlinear vertical displacement behaviour of the dam as compared with the far-fault earthquake.

6.3 Horizontal displacement results

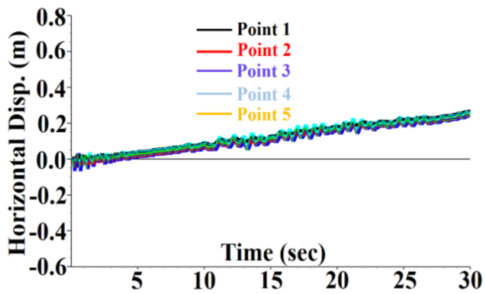

(a) Far-fault earthquake analysis results

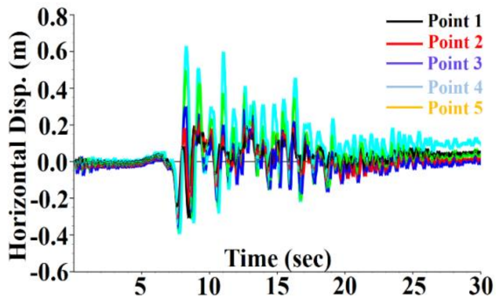

(b) Near-fault earthquake analysis results

Fig. 25 Horizontal displacement results for 50 m of the reservoir water height

In this section, horizontal displacement results for 4 various reservoir conditions are shown considering 1995 Kobe far-fault and near-fault earthquakes. Seismic analysis results are graphically presented in Figs. 24-27. Moreover, five various nodal points are selected on the dam body surface, and horizontal displacements of these critical points are shown in the graphics. According to Fig. 24(a), horizontal displacements for empty reservoir condition are presented considering the far-fault earthquake. 0.3 m maximum displacement is observed at Point 4, and

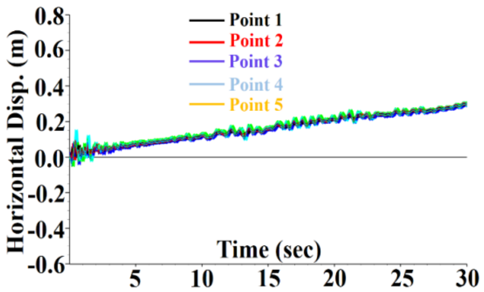

(a) Far-fault earthquake analysis results

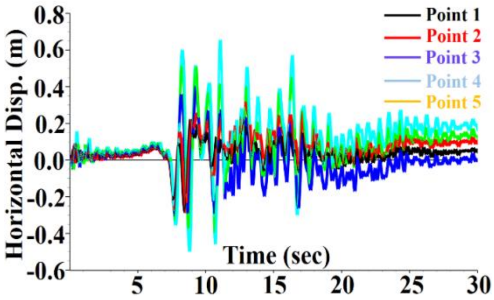

(b) Near-fault earthquake analysis results

Fig. 26 Horizontal displacement results for 100 m of the reservoir water height

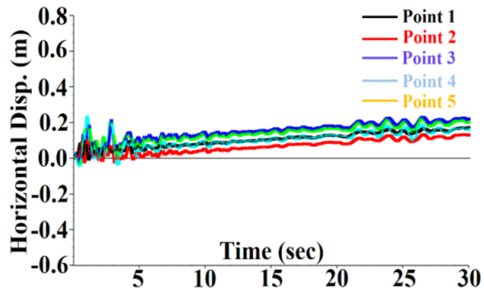

(a) Far-fault earthquake analysis results

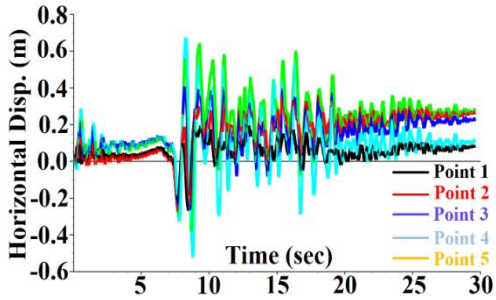

(b) Near-fault earthquake analysis results

Fig. 27 Horizontal displacement results for 130 m of the reservoir water height

minimum displacement occurred at Point 3. In Fig. 24(b), horizontal displacements for empty reservoir condition are shown for near-fault earthquake. When compared Fig. 24(a) and 24(b), significant displacement differences are seen, and more horizontal displacements are observed for near-fault earthquake. 0.67 m maximum horizontal displacement occurred at Point 4 at 7th second of the earthquake, and minimum displacement is observed at Point 1. During first 7 seconds, no significant horizontal displacements occurred at the dam body surface as seen Fig. 24(b). In Fig. 25(a), horizontal displacement results for 50 m of the reservoir water height is graphically shown taking into account far-fault earthquake. Maximum displacement is observed at Point 4, and minimum displacement occurred at Point 3. According to Fig. 25(b), horizontal displacement results for 50 m of reservoir water height are presented for near-fault earthquake. 0.64 m maximum horizontal displacement is observed at Point 4, and minimum displacement occurred at Point 1 (lowest point). When compared Fig. 24(b) and 25(b), it is clearly seen that the direction of the horizontal displacements changes from the negative direction to positive direction. This result is clearly shown the effect of the hydrostatic pressure on the horizontal displacement behaviour of the CFR dams.

In Fig. 26(a), horizontal displacements for 100 m of the reservoir water height are shown considering far-fault earthquake. Maximum horizontal displacement is observed at Point 4, and minimum displacement occurred at Point 3. According to Fig. 26(b), near-fault earthquake results are presented for 100 m of reservoir water height. 0.68 m maximum horizontal displacement occurred at Point 4, and minimum displacement is observed at Point 1. In addition, in Fig. 27(a), displacement results for 130 m of the reservoir water height (full reservoir condition) are shown considering far-fault earthquake. Maximum horizontal displacement is observed at Point 3, and minimum displacement occurred at Point 2. Finally, when examined near-fault earthquake analysis results for full reservoir condition (Fig. 27(b)), maximum displacement is observed at Point 5, and minimum horizontal displacement occurred at Point 1. These results are shown that as reservoir water height increase, horizontal displacement behaviour of the dam is clearly change. Moreover, more horizontal displacements are observed for near-fault earthquake when compared far-fault earthquake.

7. Conclusions

In this paper, the nonlinear seismic behaviour of Ilısu dam is examined for 1995 Kobe near and far-fault earthquakes considering the dam body-foundation-concrete slab interaction condition. While defining these interaction conditions to the 3D model, special interaction parameters are calculated, and they are defined to the 3D model using the special fish functions. As a consequence, interaction conditions between dam body-concrete slab and dam body-foundation are obtained. The three dimensional (3D) finite difference model of the Ilısu dam is created according to the original dam project. While creating the 3D model, Mohr Coulomb and Drucker Prager nonlinear material models are used for the rockfill materials and concrete slab, respectively. In addition, special seismic boundary conditions (free field and quiet boundary conditions) that were rarely used for the CFR dams in the past, are defined the 3D finite difference model of Ilısu dam. So, this paper is very important to assess the effect of these special boundary conditions on the seismic behaviour of the dam. While performing the seismic analyses, earthquake accelerations are applied to the bottom of the 3D model using special fish functions. Total 4 different reservoir water heights are taken into account for the seismic analyses. These water heights are empty water condition, 50 m, 100 m and 130 m (full reservoir condition), respectively. Therefore, 4 various nonlinear earthquake analyses are performed for the near and far-fault earthquakes. The effects of various reservoir water heights on the nonlinear earthquake behaviour of the Ilısu dam is evaluated as below:

- The effect of reservoir water height on the nonlinear seismic behaviour of Ilısu dam is clearly seen in this paper. According to all earthquake results, maximum principal stress is observed for 130 m of the reservoir water height (full reservoir condition), and minimum principal stress occurred for the empty reservoir condition of the dam. As the reservoir water height increase, the nonlinear seismic stress behaviour of Ilısu dam clearly changes. Moreover, when compared five various nodal points on the dam body surface with each other, maximum principal stress is observed at the lowest nodal points (nodal point 2) of the dam body surface due to the effect of the hydrostatic pressure, and minimum stress occurred at the top nodal points (nodal point 4) of the dam body surface.
- In this study, very special seismic boundary conditions that were rarely used to examined CFR dam's seismic behaviour, is used in the numerical analyses. According to earthquake analysis results, the effect of the free field and quiet boundary conditions on the nonlinear dynamic behaviour of Ilısu CFR dam is clearly seen.
- When reservoir water increases, the vertical displacement behaviour of the dam is obviously changes. According to the seismic analysis results, maximum settlements are observed for full reservoir condition of the dam, and minimum settlement is occurred for empty reservoir condition. In addition, during the earthquake analyses, -0.54 m maximum vertical displacement is observed at nodal point 4 for 130 m of the reservoir water height, and minimum displacement occurred at nodal point 3 and nodal point 2. This result is very important to evaluate the effect of increases in seasonal reservoir water level on the nonlinear seismic settlement behaviour of Ilısu dam.
- According to horizontal displacement results, as reservoir water height rise, horizontal displacements obviously increase. Maximum horizontal displacements are observed at full reservoir condition, and minimum displacements occurred at the empty reservoir condition. In addition, maximum horizontal displacements are observed at Point 4, and minimum displacements occurred at Point 1 (lowest nodal point).
- When compared the near-fault and far-fault earthquake analysis results, more principal stresses, horizontal displacements and vertical displacement values are observed on the dam body surface for the near-fault earthquake. In other word, near-fault earthquakes create more significant seismic effects on the nonlinear earthquake behaviour of Ilısu CFR dam as compared with the far-fault earthquake.

References

Bayraktar, A. and Kartal, M.E. (2010), "Linear and nonlinear response of concrete slab on CFR dam during earthquake", *Soil Dyn. Earthq. Eng.*, **30**(10), 990-1003.

Bayraktar, A., Kartal, M.E. and Adanur, S. (2011), "The effect of concrete slab-rockfill interface behavior on the earthquake performance of a CFR dam", *Int. J. Nonlin. Mech.*, **46**, 35-46.

Bayraktar, A., Kartal, M.E. and Basaga, H.B. (2009), "Reservoir water effects on earthquake performance evaluation of Torul Concrete Faced Rockfill Dam", *Water Sci. Eng.*, **2**(1), 43-57.

Cen, W., Wen, L., Zhang, Z. and Xiong, K. (2016), "Numerical simulation of seismic damage and cracking of concrete slabs of high concrete face rockfill dams", *Water Sci. Eng.*, **9**(3), 205-211.

Chen, S., Fu, Z., Wei, K. and Han, H. (2016), "Seismic responses of high concrete face rockfill dams: A case study", *Water Sci. Eng.*, **9**(3), 195-204.

Cooke, J.B. (1984), "Progress in rock-fill dams, (18th Terzaghi Lecture)", *J. Geotech. Eng.*, ASCE, **110**(10), 1381-1414.

Dakoulas, P. (2012), "Nonlinear seismic response of tall concrete-faced rockfill dams in narrow canyons", *Soil Dyn. Earthq. Eng.*, **34**, 11-24.

DSI (2018) General Directorate of State Hydraulic Works, Regional Directorate, Ankara.

Han, B., Zdravkovic, L., Kontoe. S. and Taborda, D. (2016), "Numerical investigation of the response of the Yele rockfill dam during the 2008 Wenchuan earthquake", *Soil Dyn. Earthq. Eng.*, **88**, 124-142.

Itasca Consulting Group, Inc. (2002), FLAC Version 5 user manual. Minneapolis, USA: Itasca Consulting Group, Inc.

Karalar, M. and Çavuşli, M. (2018), "Effect of normal and shear interaction stiffnesses on three-dimensional viscoplastic creep behaviour of a CFR dam", *Adv. Civil Eng.*, **2018**, Article ID 2491652.

Kartal, M.E., Cavusli, M. and Sunbul, A.B. (2017), "Assessing seismic response of a 2D roller-compacted concrete dam under variable reservoir lengths", *Arab. J. Geosci.*, **10**, 488.

Kong, X., Zhang, Y., Zou, D., Qu, Y. and Yu, X. (2017), "Seismic cracking analyses of two types of face slab for concrete-faced rockfill dams", *SCIENCE CHINA Technol. Sci.*, **60**(4), 510-522.

Noorzad, R. and Omidvar, M. (2010), "Seismic displacement analysis of embankment dams with reinforced cohesive shell", *Soil Dyn. Earthq. Eng.*, **30**, 1149-1157.

Seiphoori, A., Haeri, S.M. and Karimi, M. (2011), "Three dimensional nonlinear seismic analysis of concrete faced rockfill dams subjected to scattered P, SV, and SH waves considering the dam-foundation interaction effects", *Soil Dyn. Earthq. Eng.*, **31**, 792-804.

Xu, B., Zhou, Y. and Zou, D. (2014), "Numerical simulation on slabs dislocation of zipingpu concrete faced rockfill dam during the Wenchuan earthquake vased on a generalized plasticity model", *Scientif World J.*, **2014**, Article ID 572407.

Xu, B., Zou, D. and Liu, H. (2012), "Three-dimensional simulation of the construction process of the Zipingpu concrete face rock-fill dam based on a generalized plasticity model", *Comput. Geotech.*, **43**, 143-154.

Xu, B., Zou, D., Kong, X., Hu, Z. and Zhou, Y. (2015), "Dynamic damage evaluation on the slabs of the concrete faced rockfill dam with the plastic-damage model", *Comput. Geotech.*, **65**, 258-265.

Xu, H., Zou, D., Kong, X. and Hu, Z. (2016), "Study on the effects of hydrodynamic pressure on the dynamic stresses in slabs of high CFRD based on the scaled boundary finite-element method", *Soil Dyn. Earthq. Eng.*, **88**, 223-236.

Xu, H., Zou, D., Kong. X., Hu, Z. and Su, X. (2018), "A nonlinear analysis of dynamic interactions of CFRD compressible reservoir system based on FEM-SBFEM", *Soil Dyn. Earthq. Eng.*, **112**, 24-34.

Yamaguchi, Y., Kondo, M. and Kobori, T. (2012), "Safety inspections and seismic behavior of embankment dams during the 2011 off the Pacific Coast of Tohoku earthquake", *Soil. Found.*, **52**(5), 945-955.

Zou, D., Han, H., Liu. J., Yang, D. and Kong, X. (2018), "Seismic failure analysis for a high concrete face rockfill dam subjected to near-fault pulse-like ground motions", *Soil Dyn. Earthq. Eng.*, **98**, 235-243.

Zou, D., Xu, B., Kong, X., Liu, H. and Zhou, Y. (2013), "Numerical simulation of the seismic response of the Zipingpu concrete face rockfill dam during the Wenchuan earthquake based on a generalized plasticity model", *Comput. Geotech.*, **49**, 111-122.

AT